A Standard Compatible Forward Error Correction Extension for the Automatic Identification System

Armin Dammann, Ronald Raulefs and Markus Wirsing

***Abstract*—The Automatic Identification System (AIS) is important for collision avoidance in maritime traffic but does not provide error correction mechanisms for erroneous transmissions. In this document we propose and study a standard compatible forward error correction (FEC) extension for the AIS. The AIS standard defines Gaussian minimum shift keying (GMSK) modulation, an easy to implement modulation scheme with constant envelope, which carries information solely in its phase. We propose to extend GMSK to multi-amplitude Gaussian minimum shift keying (MA-GMSK) modulation. MA-GMSK can be processed by off-the-shelf AIS receivers, thus ensuring standard compatibility. Additionally, with MA-GMSK we transmit additional bits via amplitude modulation, which we use to transmit redundancy bits for FEC. We evaluate the AIS packet error rate (PER) performance when modifying the AIS by FEC. We examine the AIS PERs when applying appropriate demodulation and decoding at an advanced AIS receiver. In order to verify standard compatibility, we investigate the PER performance of common-off-the-shelf AIS receivers, which are fed with an MA-GMSK signal. Based on simulation and measurement results, we propose an MA-GMSK amplitude modulation coefficient of $\Delta A = 0.4$. With this choice, common-off-the-shelf AIS receivers provide a PER performance close to the standard reference, i.e., GMSK modulation. At the same time performance improvements between 1.3 and 3 dB provided by an advanced receiver, applying FEC as proposed in this document, are preserved.**

***Index Terms*— Automatic Identification System (AIS), Convolutional Code, forward error correction (FEC), Gaussian minimum shift keying (GMSK), multi-amplitude Gaussian minimum shift keying (MA-GMSK), Mutual Information, standard compatibility, Turbo Code**

I. Introduction

GAUSSIAN minimum shift keying (GMSK) modulation has been used by a variety of mobile radio communication systems. Well known standards, applying GMSK modulation, are the Global System for Mobile Communications (GSM) [1,2], Digital Enhanced Cordless Telecommunications (DECT) [3,4], Bluetooth Low Energy (BLE) [5] or the Automatic Identification System (AIS) [6].

Using GMSK modulation is often justified by its low implementation complexity at both transmitter and receiver, the compact spectrum and, in particular, its constant envelope. Due to a constant signal envelope, GMSK allows power amplifiers to operate close to their optimum operating point in terms of power efficiency. However, constant envelope signals like GMSK make inefficiently use of the entire signal space. In baseband, a GMSK signal varies on the unit circle, thus containing information modulated onto its phase only.

Our aim is to apply amplitude modulation as a further degree of freedom for the transmission of additional data, while keeping the original modulation of the phase as undistorted as possible. The extension of a GMSK system standard by applying multi-amplitude Gaussian minimum shift keying (MA-GMSK) while retaining the original phase modulation properties of GMSK provides standard compatibility.

MA-GMSK increases compared to GMSK the spectral efficiency. Our goal is to transmit data which is redundant to data which is transmitted using the standard compatible phase modulation capabilities. We exploit the redundancy for forward error correction (FEC) by applying appropriate channel coding. Especially for systems without FEC, such as the AIS, MA-GMSK is a suitable possibility to implement FEC retroactively and compatible to the original standard.

A. Organization of this Document

In Sec. II, we introduce the implementation of the continuous phase modulation (CPM) schemes minimum shift keying (MSK) and its modification GMSK. GMSK modulation is the main building block of MA-GMSK. MA-GMSK modulation as a weighted superposition of two GMSK modulated signals is introduced in Sec. II-C.

In Sec. III we present maximum a-posteriori (MAP) demodulation methods for GMSK. These demodulation schemes provide soft-decision values for each bit in form of log-likelihood ratios (LLRs). These LLRs are used as input for soft-decision for a FEC decoding algorithm.

MA-GMSK modulation introduces a parameter ΔA — we call it the *amplitude modulation coefficient* — which controls the Euclidean distance of the two amplitude levels of our MA-GMSK modulation scheme. In Sec. IV we investigate the influence of the amplitude modulation coefficient on the achievable information throughput when applying MA-GMSK modulation. We aim to find an amplitude modulation coefficient ΔA, which provides an information throughput as high as possible. We measure information throughput in terms of *mutual information* between transmitted bits and the corresponding LLR at the output of the MA-GMSK modulator. An approach how to measure mutual information from LLRs is shown in Appendix A.

The authors are with the Institute of Communications and Navigation, German Aerospace Center (DLR), Oberpfaffenhofen, Muenchner Str. 20, 82234 Wessling, Germany, Email: {firstname.lastname}@DLR.de

In Sec. V we describe how to modify the AIS by FEC in a standard compatible manner. Standard compatibility means that after this modification, a common-off-the-shelf AIS receiver is still able to work within specifications, even when operated with the modified AIS. An advanced AIS receiver, however, exploits the additional FEC capabilities for improving the AIS packet error rate (PER) performance. Appropriate FEC coding schemes, in particular turbo coding and convolutional coding, are introduced in Sec. V-B.

In Sec. VI we evaluate the AIS PERs when applying appropriate demodulation and decoding at an advanced AIS receiver. In order to verify standard compatibility, we investigate the packet error rate (PER) performance of common-off-the-shelf AIS receivers, which are fed with an multi-amplitude Gaussian minimum shift keying (MA-GMSK) signal.

In Sec. VII we summarize this study and draw the conclusions.

B. A Quick Path Through this Document

For quickly getting the idea, approach and results for standard compatible FEC extension of the AIS the reader might skip the introduction to basics about the individual building blocks. Being familiar with GMSK modulation, the reader might directly continue with Sec. II-C, where we explain the implementation of multi-amplitude Gaussian minimum shift keying (MA-GMSK) modulation based on GMSK. Next, the reader might proceed to the introduction to Sec. V and subsection V-A. These paragraphs explains how to apply the proposed standards-compliant FEC extension to AIS. Finally, the AIS PER results from computer simulations and laboratory measurements can be found in Sec. VI.

II. Continuous Phase Modulation

In this section, we briefly introduce binary CPM. Detailed introductions into CPM can be found in many textbooks, e.g. [7, Sec. 3.3.2]. The complex valued base band signal

$$s(t) = \exp\left(\jmath\,\Phi(t)\right) \tag{1}$$

has a constant envelope. Its phase

$$\Phi(t) = 2\pi\,h\sum_{n=-\infty}^{+\infty} x_n\,q(t-n\,T) \tag{2}$$

carries the information the transmitted bits $x_n \in \{+1,-1\}$. One information bit is transmitted in a time interval of duration T. The Parameter h is called the *modulation index*. The phase response

$$q(t) = \int_0^t u(\tau)\;\mathrm{d}\tau \tag{3}$$

can be constructed by integration from a frequency response pulse $u(t)$, where $u(t) = 0$ for $t < 0$ and $\lim_{t\to\infty} q(t) = \frac{1}{2}$. The case $u(t) = 0$ for $t > T$, meaning that the entire phase change for one information bit occurs during one time interval of duration T, is called *full response CPM*. The other case $u(t) \neq 0$ for $t > T$, is called *partial response CPM*.

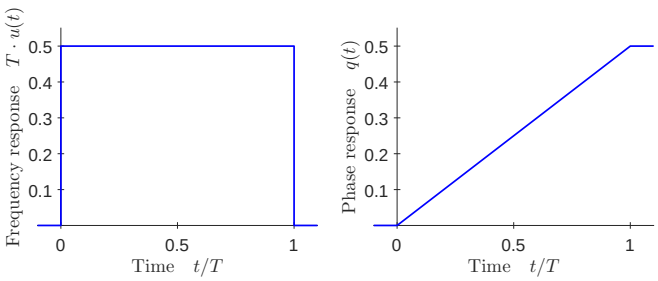

(a) Frequency response. (b) Phase response.

Fig. 1: MSK: frequency and phase responses.

A. Minimum Shift Keying (MSK)

A well-known representative of a full response CPM modulation scheme is MSK. Its modulation index $h = 1/2$, meaning that the phase of the baseband signal changes by $\pm\pi/2$, depending on the corresponding information bit $x_n \in \{-1,+1\}$. The frequency response pulse $u(t) = \frac{1}{2\,T}$ for $0 \le t \le T$ is constant during the time interval $[0,T]$. This leads to a phase response which is linearly increasing from $q(0) = 0$ to $q(T) = 1/2$. Fig. 1 shows frequency and phase response for MSK. MSK is equivalent to offset quadrature phase shift keying (OQPSK) with half-sinusoid pulse shaping [8]. It therefore belongs to the linear modulation schemes as well. Due to its discontinuous frequency response, MSK shows a broad power density spectrum (PDS). One approach to get a more narrow PDS is to low-pass filter the rectangular frequency response pulse $u(t)$. This filtering results in smoother frequency and phase response functions. However, they last over more than one symbol interval T, leading to partial response CPM. One representative of a partial response CPM scheme is Gaussian minimum shift keying (GMSK), which we are going to introduce in the next section.

B. Gaussian Minimum Shift Keying (GMSK)

Gaussian minimum shift keying (GMSK) is a representative of the partial response CPM schemes. The frequency response pulse

$$\begin{aligned}\tilde{u}(t) &= u_0(t) * h_{\mathrm{G}}(t)\\ &= \int_{-\infty}^{\infty} u_0(t-\tau) * h_{\mathrm{G}}(\tau)\;\mathrm{d}\tau = \frac{1}{2\,T}\int_{t-\frac{T}{2}}^{t+\frac{T}{2}} h_{\mathrm{G}}(\tau)\;\mathrm{d}\tau\\ &= \frac{1}{4\,T}\left[\operatorname{erf}\left(\pi\,(BT)\sqrt{\frac{2}{\ln 2}}\left(\frac{t}{T}+\frac{1}{2}\right)\right)\right.\\ &\qquad\left.-\operatorname{erf}\left(\pi\,(BT)\sqrt{\frac{2}{\ln 2}}\left(\frac{t}{T}-\frac{1}{2}\right)\right)\right]\end{aligned} \tag{4}$$

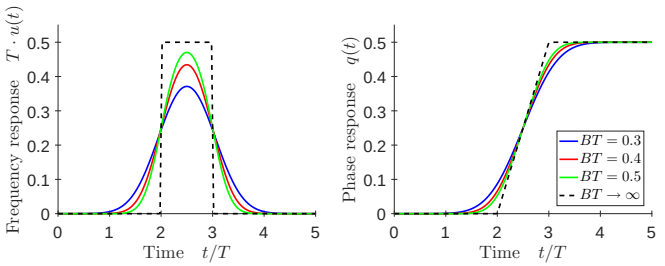

(a) Frequency response. (b) Phase response.

Fig. 2: GMSK: frequency and phase responses for different normalized Gaussian low-pass filter bandwidths BT.

of GMSK is obtained by passing a rectangular pulse

$$u_0(t) = \begin{cases} \frac{1}{2T}, & -\frac{T}{2} \le t \le \frac{T}{2} \\ 0, & \text{else} \end{cases} \tag{5}$$

of duration T through a Gaussian low-pass filter with a 3 dB-bandwidth of B. The Gaussian low-pass filter impulse response is

$$h_{\mathrm{G}}(t) = \frac{(BT)}{T}\sqrt{\frac{2\pi}{\ln 2}}\exp\left(-\frac{2\pi^2(BT)^2}{\ln 2}\left(\frac{t}{T}\right)^2\right). \tag{6}$$

For notational convenience we consider the pulses $u_0(t)$ and $h_{\mathrm{G}}(t)$ being symmetric with respect to $t = 0$. The Gaussian low-pass filter impulse response and consequently also the frequency response pulse $\tilde{u}(t)$ have an infinite temporal expansion. In practical systems such a frequency response pulse is not realizable. Depending on the normalized bandwidth BT, most of the energy of the frequency response pulse is concentrated within an interval of L symbols. This interval has a duration of LT. For practical realization, we crop the symmetric frequency response pulse $\tilde{u}(t)$ in a time interval of $[-LT/2, +LT/2]$, normalize such that the cropped pulse integrates to $1/2$ and shift the cropped and normalized pulse by $LT/2$ in order to get a causal frequency response pulse

$$u(t) = \begin{cases} \frac{1}{2c}\,\tilde{u}\left(t - \frac{LT}{2}\right), & 0 \le t \le LT \\ 0, & \text{else} \end{cases} \tag{7}$$

with normalization constant

$$c = \int_{-\frac{LT}{2}}^{+\frac{LT}{2}} \tilde{u}(t)\ \mathrm{d}t. \tag{8}$$

The phase response is calculated according to Eq. (3). Fig. 2 shows the frequency response pulses and the corresponding phase responses for $L = 5$ and different normalized Gaussian low-pass filter bandwidths BT. The graphs are normalized to the symbol duration T. For $BT \to \infty$, the GMSK frequency and phase responses are equivalent to MSK. Fig. 3 shows a MSK and a GMSK signal in the complex signal space. Black markers indicate the MSK resp. GMSK signal at integer multiples of symbol time T. At those time instants the MSK

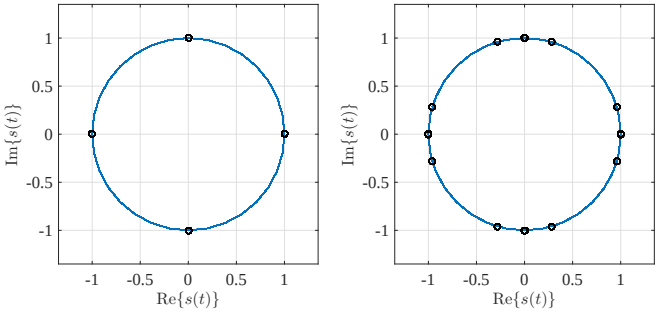

(a) MSK (b) GMSK with normalized Gaussian low-pass filter bandwidths $BT = 0.4$ and phase response length $L = 5$

Fig. 3: Signal space diagrams for MSK and GMSK.

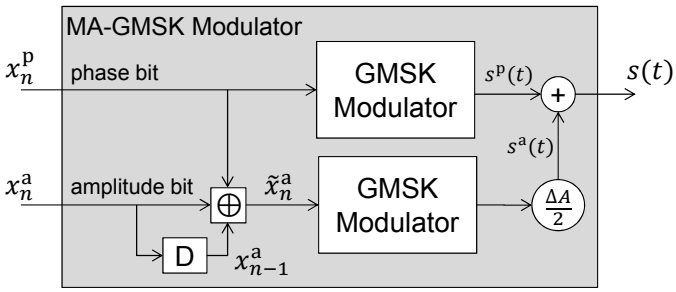

Fig. 4: MA-GMSK modulator composed of 2 GMSK modulators.

signal states show 4 dedicated values $e^{jk\frac{\pi}{2}}, k = 0, 1, 2, 3$. We observe inter-symbol interference for GMSK due to its partial phase response.

C. Multi-Amplitude GMSK

GMSK is a constant envelope modulation scheme. The entire transmitted information is contained in the phase of a GMSK signal. On the one hand a constant envelope signal allows power amplifiers at a transmitter to operate close to their optimum operating point with respect to power efficiency. On the other hand, a constant envelope signal dispenses with the possibility to use the signal space in the best possible way.

Our aim is to apply amplitude modulation as a further degree of freedom for the transmission of additional information, while keeping the original modulation of the phase as undistorted as possible. Extending a system standard by applying MA-GMSK but maintaining the original phase modulation properties of GMSK provides standard compatibility.

Rather than just multiplying a GMSK signal with a real valued amplitude modulation function, we construct an MA-GMSK signal by an appropriate superposition of 2 component GMSK signals as shown in the block diagram in Fig. 4. Constructing the signal by superposition, offers the advantage that the PDS of the MA-GMSK signal remains unchanged compared to a GMSK signal. So, compliance with given spectral masks is inherently achieved by that construction. In

TABLE I: Table of values for binary (modulo-2) addition $\oplus$ for different binary alphabet notations.

$\oplus$	+1	-1
+1	+1	-1
-1	-1	+1

$\oplus$	0	1
0	0	1
1	1	0

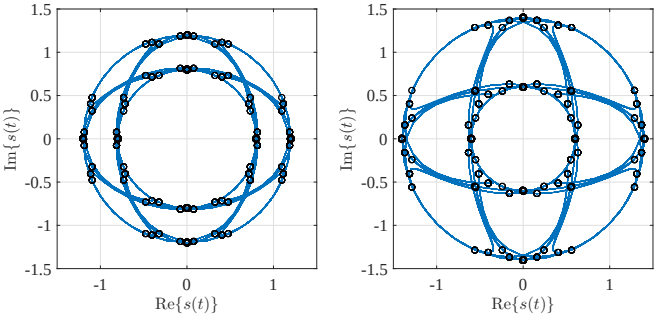

(a) $\Delta A = 0.4$ (b) $\Delta A = 0.8$

Fig. 5: Signal space diagrams for MA-GMSK with $BT = 0.4$ and different amplitude modulation coefficients ΔA.

the following we focus on a binary modulation of the GMSK signal's amplitude. With that we can transmit an additional data bit during one symbol time interval of length T. A description of multi-amplitude CPM, providing a generalization to more than 2 amplitude levels, can be found in [7, Sec. 3.3.2].

As in classical GMSK the approach shown in Fig. 4 uses a binary data symbol $x_n^{\mathrm{p}} \in \{+1, -1\}$, let's call it the *phase bit*, as input of a GMSK modulator, which provides a complex valued GMSK baseband signal $s^{\mathrm{p}}(t)$ of constant amplitude 1. The idea is now to use a second GMSK modulator, which provides a GMSK signal $s^{\mathrm{a}}(t)$ with a smaller amplitude of $\Delta A/2$ compared to the phase bit GMSK modulator. This GMSK modulator runs either in-phase or out-of-phase, with a phase shift of $\pi\,\mathrm{rad}$, compared to the phase bit GMSK modulator, depending on the *amplitude bit* $x_n^{\mathrm{a}} \in \{+1, -1\}$. Let's assume that data transmission starts at time index $n = 0$ with identical internal states of the GMSK modulators, meaning they are running in-phase at the beginning. The relative signal phase between $s^{\mathrm{p}}(t)$ and $s^{\mathrm{a}}(t)$ changes from in-phase to out-of-phase and vice versa whenever the amplitude bit changes its value. In order to achieve this we generate the input to the amplitude GMSK modulator as

$$\tilde{x}_n^{\mathrm{a}} = x_n^{\mathrm{p}} \oplus x_n^{\mathrm{a}} \oplus x_{n-1}^{\mathrm{a}}, \quad n = 0, 1, \ldots \tag{9}$$

with $x_{-1}^{\mathrm{a}} = +1$ and modulo-2 addition $\oplus$ as defined in Table I. The MA-GMSK signal

$$s(t) = s^{\mathrm{p}}(t) + s^{\mathrm{a}}(t) \tag{10}$$

is shown in Fig. 5 in the complex signal space for different amplitude modulation coefficients ΔA. From Fig. 5 we can clearly observe 2 amplitude levels and the transitions

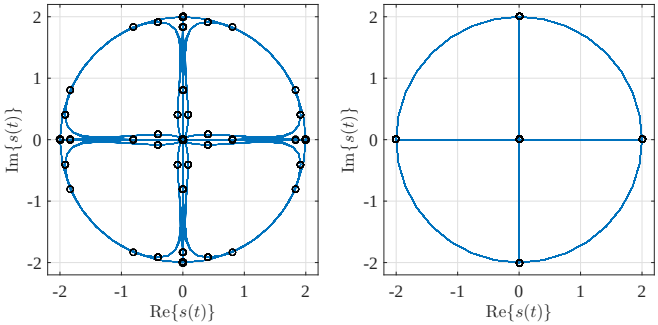

(a) $BT = 0.4$ (b) $BT \to \infty$ (MA-MSK)

Fig. 6: Signal space diagrams for MA-GMSK with maximum amplitude modulation coefficient $\Delta A = 2$.

between them. The black markers indicate the MA-GMSK signal states at integer multiples of symbol time T. The amplitude modulation coefficient ΔA is the difference of the 2 amplitude levels. Compared to GMSK, we observe additional inter-symbol interference also in amplitude direction. Note the MA-GMSK signal according to Eq. (10) is not normalized to an average power of 1.

For $\Delta A = 0$, MA-GMSK is equivalent to GMSK as shown in Fig. 3b. In this case, the MA-GMSK modulator signal $s(t)$ does not depend on amplitude bit x_n^{a}. For the maximal value $\Delta A = 2$, the inner amplitude level collapses to the origin of the complex signal plane. Fig. 6a shows the signal space diagram for MA-GMSK with $\Delta A = 2$ and $BT = 0.4$. We can observe the collapsed signal states at the origin but also significant inter-symbol interference. For comparison, Fig. 6b shows the signal space diagram for $\Delta A = 2$ and $BT \to \infty$, which means that the MA-GMSK component modulators are full response MSK modulators. In this case, the four outer amplitude level states and the collapsed inner amplitude levels are clearly visible.

III. MA-GMSK Demodulation

We sample the complex valued baseband signal $s(t)$ at the output of the MA-GMSK modulator with a rate of K samples per symbol time T. The transmitted complex valued baseband samples are $s_k = s\left(k \cdot T/K\right)$. The MA-GMSK modulator provides a one-to-one mapping between a $2N$ bit data sequence $\mathbf{x} = \left[x_0^{\mathrm{p}}, x_0^{\mathrm{a}}, x_1^{\mathrm{p}}, x_1^{\mathrm{a}}, \ldots, x_{N-1}^{\mathrm{p}}, x_{N-1}^{\mathrm{a}}\right]$ and the complex valued baseband sequence $\mathbf{s}(\mathbf{x}) = [s_0(\mathbf{x}), s_1(\mathbf{x}), \ldots, s_{NK-1}(\mathbf{x})]$ of length NK. At the receiver side, we observe the complex valued baseband sequence $\mathbf{r} = [r_0, r_1, \ldots, r_{NK-1}]$ of length NK.

A. MAP Demodulation

Following the symbol-by-symbol MAP approach [9,10], the MA-GMSK modulator calculates a LLR

$$L_n = \ln \frac{\mathrm{p}\left(x_n = +1|\mathbf{r}\right)}{\mathrm{p}\left(x_n = -1|\mathbf{r}\right)} = \ln \frac{\sum\limits_{\substack{\mathbf{x}\in\mathcal{X}\\ x_n=+1}} \mathrm{p}\left(\mathbf{s}(\mathbf{x})|\mathbf{r}\right)}{\sum\limits_{\substack{\mathbf{x}\in\mathcal{X}\\ x_n=-1}} \mathrm{p}\left(\mathbf{s}(\mathbf{x})|\mathbf{r}\right)} \tag{11}$$

for each of the $2N$ bits in data sequence $\mathbf{x}$ given the received complex baseband sequence $\mathbf{r}$. Set $\mathcal{X}$ contains all possible data sequences $\mathbf{x} = \left[x_0^{\mathrm{p}}, x_0^{\mathrm{a}}, x_1^{\mathrm{p}}, x_1^{\mathrm{a}}, \ldots, x_{NK-1}^{\mathrm{p}}, x_{NK-1}^{\mathrm{a}}\right]$ at the input of the MA-GMSK modulator. The cardinality of set $\mathcal{X}$ is $|\mathcal{X}| = 2^{2N}$. By applying Bayes' rule, Eq. (11) can be rewritten to

$$L_n = \ln \frac{\mathrm{p}(x_n = +1)}{\mathrm{p}(x_n = -1)} + \ln \sum_{\substack{\mathbf{x}\in\mathcal{X}\\ x_n=+1}} \mathrm{p}\left(\mathbf{r}|\mathbf{s}(\mathbf{x})\right) - \ln \sum_{\substack{\mathbf{x}\in\mathcal{X}\\ x_n=-1}} \mathrm{p}\left(\mathbf{r}|\mathbf{s}(\mathbf{x})\right). \tag{12}$$

The first right hand side term of Eq. (12) is the a priori LLR for data bit x_n. It equals 0 for data bits with equal probability $\mathrm{p}(x_n = +1) = \mathrm{p}(x_n = -1) = 0.5$.

Assuming statistical independence of the likelihood function, i.e., $\mathrm{p}\left(\mathbf{r}|\mathbf{s}(\mathbf{x})\right) = \prod_k \mathrm{p}\left(r_k|s_k(\mathbf{x})\right)$ yields

$$L_n = \ln \frac{\mathrm{p}(x_n = +1)}{\mathrm{p}(x_n = -1)} + \ln \sum_{\substack{\mathbf{x}\in\mathcal{X}\\ x_n=+1}} \prod_{k=0}^{NK-1} \mathrm{p}\left(r_k|s_k(\mathbf{x})\right) - \ln \sum_{\substack{\mathbf{x}\in\mathcal{X}\\ x_n=-1}} \prod_{k=0}^{NK-1} \mathrm{p}\left(r_k|s_k(\mathbf{x})\right). \tag{13}$$

B. Log-MAP Demodulation

In Eq. (13) many likelihoods $\mathrm{p}\left(r_k|s_k(\mathbf{x})\right)$ are close to zero, especially for good channel conditions with low noise. This can cause numerical inaccuracies when calculating the sum-product terms. In order to prevent such numerical problems it is preferable to use logarithmic likelihoods $\ln \mathrm{p}\left(r_k|s_k(\mathbf{x})\right)$. Thus, we aim to bring the logarithm operation inside the sum-product in Eq. (13). For the product this can be achieved by applying the logarithmic calculus rules. Exchanging the logarithm operation and summation, however, is not that straightforward. Following [10] we express the logarithm of a sum of probabilities p_1 and p_2

$$\log\left(p_1 + p_2\right) = \max\left(\log p_1, \log p_2\right) + \log\left(\mathrm{e}^{-|\log p_1 - \log p_2|} + 1\right) \tag{14}$$

by taking the maximum of the logarithmic probabilities and applying a correction term. For more than two addends, which is very likely the case in Eq. (13), we apply Eq. (14) recursively. We abbreviate this operation with a *'boxsum'*

$$\boxplus_n \log p_n := \log \sum_n p_n \tag{15}$$

and rewrite Eq. (13) to

$$L_n = \ln \frac{\mathrm{p}(x_n = +1)}{\mathrm{p}(x_n = -1)} + \boxplus_{\substack{\mathbf{x}\in\mathcal{X}\\ x_n=+1}} \sum_{k=0}^{NK-1} \ln \mathrm{p}\left(r_k|s_k(\mathbf{x})\right) - \boxplus_{\substack{\mathbf{x}\in\mathcal{X}\\ x_n=-1}} \sum_{k=0}^{NK-1} \ln \mathrm{p}\left(r_k|s_k(\mathbf{x})\right). \tag{16}$$

This version of MAP using log-likelihoods is called logarithmic MAP (Log-MAP).

C. Max-Log-MAP Demodulation

Both, MAP and Log-MAP are optimal demodulation algorithms. Neglecting the correction term in Eq. (14) provides an approximation

$$\log \sum_n p_n \approx \max_n \log p_n \tag{17}$$

for the logarithm of a sum of probabilities. We apply this maximum logarithm approximation to Eq. (13) and arrive at maximum logarithm MAP (Max-Log-MAP) sub-optimal demodulation

$$L_n \approx \ln \frac{\mathrm{p}(x_n = +1)}{\mathrm{p}(x_n = -1)} + \max_{\substack{\mathbf{x}\in\mathcal{X}\\ x_n=+1}} \sum_{k=0}^{NK-1} \ln \mathrm{p}\left(r_k|s_k(\mathbf{x})\right) - \max_{\substack{\mathbf{x}\in\mathcal{X}\\ x_n=-1}} \sum_{k=0}^{NK-1} \ln \mathrm{p}\left(r_k|s_k(\mathbf{x})\right). \tag{18}$$

The LLRs can be efficiently calculated by the BCJR algorithm [9], which implements the sum-product structure of Eq. (13), the sum-sum structure of Eq. (16) or the max-sum structure of Eq. (18) on a trellis.

If the received complex valued baseband signal samples

$$r_k = s_k + \epsilon_k, \qquad k = 0, \ldots N\,K - 1 \tag{19}$$

are corrupted by complex valued additive white Gaussian noise (AWGN) ϵ_k with zero mean and variance $\mathrm{E}\left\{|\epsilon_k|^2\right\} = \sigma_\epsilon^2$, the likelihood function is

$$\mathrm{p}\left(r_k|s_k(\mathbf{x})\right) = \frac{1}{\sqrt{\pi\sigma_\epsilon^2}}\,\mathrm{e}^{-\frac{|r_k - s_k(\mathbf{x})|^2}{\sigma_\epsilon^2}}. \tag{20}$$

IV. Parameterization of the Amplitude Modulation Coefficient ΔA for MA-GMSK

The MA-GMSK modulator, introduced in Sec. II-C, provides us with the opportunity to transmit 2 bits at one time interval of duration T. One of these bits — the 'phase bit' in Fig. 4 — determines the phase of the complex valued signal $s(t)$, similar to classical GMSK modulation. The 'amplitude bit' influences the amplitude of $s(t)$. The amount of information, which we can transfer via the 'phase bit' respectively the 'amplitude bit' depends on the MA-GMSK amplitude modulation coefficient ΔA.

For a small ΔA the Euclidean distance between the inner and the outer signal constellation symbols is small, leading

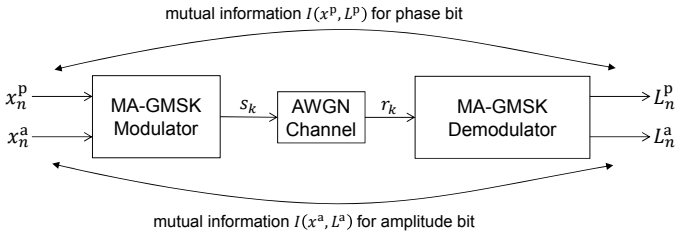

Fig. 7: Measuring mutual information between transmitted bits and MA-GMSK demodulator output.

to higher error probabilities, and therefore, lower information transfer capabilities. In particular, for $\Delta A \to 0$ the symbols become less and less distinguishable, leading to a bit error rate which tends to 0.5 and a corresponding information transfer which goes to zero. The Euclidean distances between the different phase states of the symbols approach those of classical GMSK.

With increasing ΔA the Euclidean distance between symbols with different amplitude increases as well, leading to lower bit error rate and corresponding higher information transfer in the amplitude bit. The Euclidean distances for symbols with different phase states decrease for the inner ring of symbols. This leads to an increased bit error rate, and therefore, reduced information transfer for the phase bit.

Therefore, if we increase ΔA from 0 to 2, the mutual information for the amplitude bit monotonically increases, while the mutual information for the phase bit monotonically decreases. This increase, respectively, decrease of mutual information is not proportional to ΔA. Therefore, there should be an optimal ΔA which maximizes the sum of mutual information for the phase bit and the amplitude bit.

We measure mutual information between N transmitted phase bits x_n^{p} respectively N amplitude bits x_n^{a} and their corresponding LLRs L_n^{p} respectively L_n^{a} at the receiver side as shown in Fig. 7.

A $2N$ bit data sequence

$$\mathbf{x} = \left[x_0^{\mathrm{p}}, x_0^{\mathrm{a}}, x_1^{\mathrm{p}}, x_1^{\mathrm{a}}, \ldots, x_{N-1}^{\mathrm{p}}, x_{N-1}^{\mathrm{a}}\right] \tag{21}$$

is fed into a MA-GMSK modulator. Signal $s(t)$ at the output of the MA-GMSK modulator is sampled with a rate of $K = 8$ samples per symbol time T providing a complex valued baseband transmit sequence

$$\mathbf{s}(\mathbf{x}) = [s_0(\mathbf{x}), s_1(\mathbf{x}), \ldots, s_{NK-1}(\mathbf{x})] \tag{22}$$

of length NK. The received signal samples

$$r_k = s_k + \epsilon_k, \qquad k = 0, \ldots NK-1 \tag{23}$$

are corrupted by AWGN ϵ_k with zero mean and variance $\mathrm{E}\left\{|\epsilon_k|^2\right\} = \sigma_\epsilon^2$. The signal-to-noise ratio (SNR)

$$\mathrm{SNR} = \frac{\frac{1}{NK}\sum_{k=0}^{NK-1}|s_k|^2}{\sigma_\epsilon^2} = \frac{\frac{1}{T}E_{\mathrm{s}}}{B\,N_0} = \frac{1}{K}\frac{E_{\mathrm{s}}}{N_0} \tag{24}$$

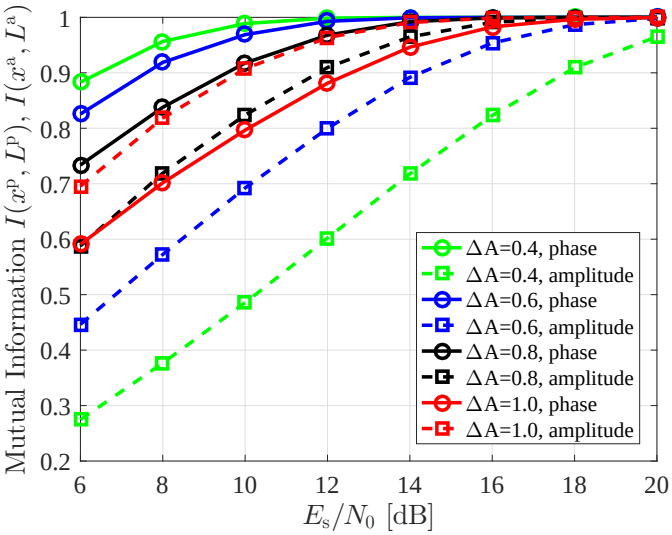

Fig. 8: Individual mutual information between transmitted phase resp. amplitude bit and the corresponding Max-Log-MAP MA-GMSK demodulator outputs versus E_{s}/N_0.

at the receiver input depends on signal energy E_{s}, noise power density N_0 and the oversampling factor K, i.e., the number of samples per symbol time, since the Nyquist bandwidth $B = K/T$ and the AWGN power $\sigma_\epsilon^2 = B\,N_0$.

We calculate the mutual information $I(x^{\mathrm{p}}, L^{\mathrm{p}})$ between N phase bits x_n^{p} and LLRs L_n^{p} respectively the mutual information $I(x^{\mathrm{a}}, L^{\mathrm{a}})$ between N amplitude bits x_n^{a} and LLRs L_n^{a} according to

$$\mathrm{I}(x; L) \approx 1 - \frac{1}{N}\sum_{n=1}^{N}\mathrm{H_b}\left(\frac{1}{1+\mathrm{e}^{-L_n}}\right). \tag{25}$$

For the derivation see Appendix A and Eq. (39) therein, where $\mathrm{H_b}\left(\mathrm{p}(x=+1)\right) = 1$ for equally probable data bits $x \in \{-1, +1\}$.

Fig. 8 shows these individual mutual information versus E_{s}/N_0 for a Max-Log-MAP MA-GMSK demodulator according to Eq. (18). With increasing amplitude modulation coefficient ΔA, the mutual information $I(x^{\mathrm{p}}, L^{\mathrm{p}})$ for the phase bit decreases whereas the mutual information $I(x^{\mathrm{a}}, L^{\mathrm{a}})$ for the amplitude bit increases. This confirms our discussion at the beginning of this section. Fig. 9a shows the total mutual information $I(x^{\mathrm{p}}, L^{\mathrm{p}}) + I(x^{\mathrm{a}}, L^{\mathrm{a}})$ versus E_{s}/N_0 for Max-Log-MAP demodulation. We observe that the total mutual information is maximized for an amplitude modulation coefficient of $\Delta A \approx 0.8$ for the entire range of considered E_{s}/N_0. For comparison Fig. 9b shows the total mutual information for Log-MAP demodulation. Comparing optimal Log-MAP and sub-optimal Max-Log-MAP demodulation, we observe that performance differences in terms of mutual information are negligible. This justifies the application of computationally lower complex Max-Log-MAP demodulation.

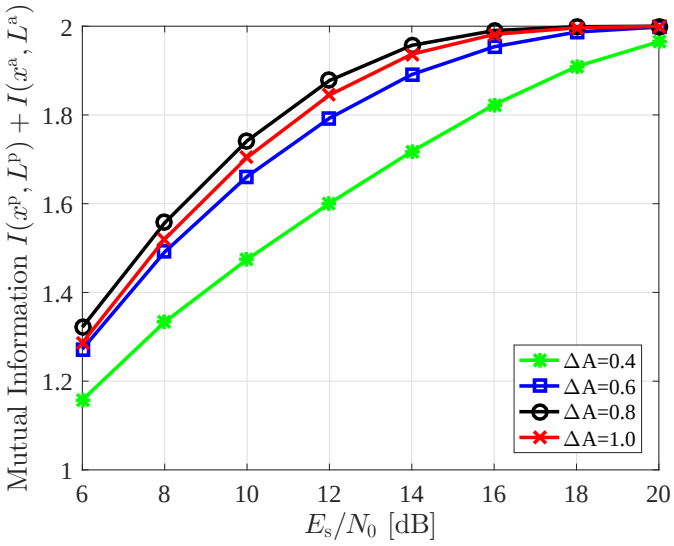

(a) Max-Log-MAP

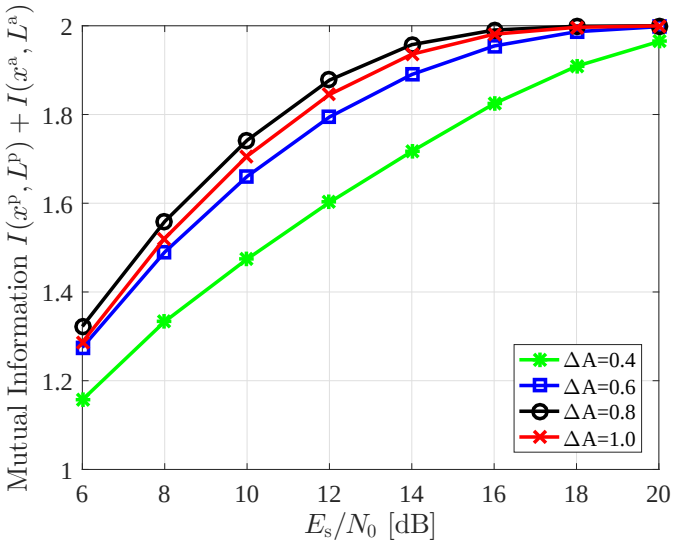

(b) Log-MAP

Fig. 9: Total (sum) mutual information between transmitted phase resp. amplitude bit and the corresponding MA-GMSK demodulator outputs versus E_{s}/N_0.

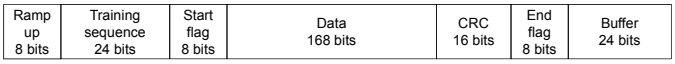

Fig. 10: 256 bit AIS data packet.

V. Application of Standard Compatible Error Protection to the AIS

AIS is a self organized time division multiple access (TDMA) (SO-TDMA) system [6]. One TDMA frame of 60 s length is divided into 2250 slots, each of length 26.67 ms. Within a slot, a 256 bit data packet is transmitted at a rate of 9600 bit/s using GMSK modulation. Fig. 10 shows the structure of an AIS data packet. One AIS data packet contains 168 data bits, followed by 16 cyclic redundancy check (CRC) bits for error detection. Besides the CRC bits no further redundancy

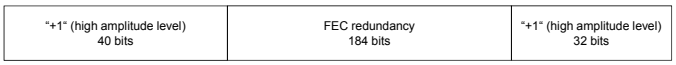

Fig. 11: The 256 amplitude bits for MA-GMSK modulation of an AIS data packet.

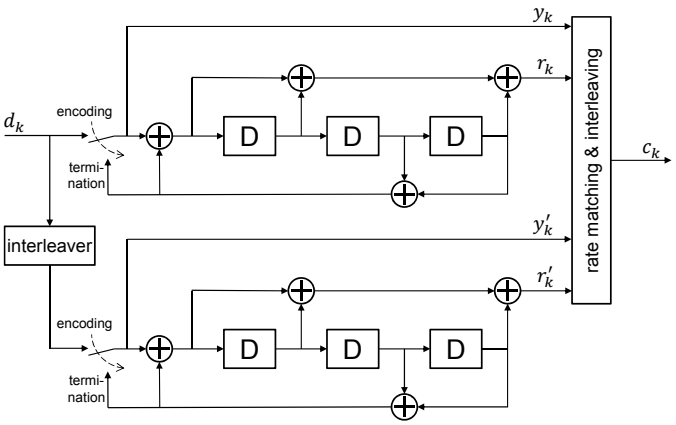

Fig. 12: LTE turbo encoder.

bits, which could be used for error correction, are transmitted.

A. The Basic Idea

In order to correct errors after transmission of an AIS data packet, we apply FEC. We use a rate-1/2 systematic channel code for encoding the data part of an AIS data packet. As shown in Fig. 10, the AIS data packet part consists of 168 data bits and 16 CRC bits. Since we use a systematic code, the 184 data bits itself appear in the encoded bit sequence together with further 184 redundancy bits. For modulation, AIS data packets according to Fig. 10 are fed as phase bits into a MA-GMSK modulator, such as shown in Fig. 4. These phase bits modulate the phase of the transmit signal and can be demodulated by a legacy AIS receiver, thus, ensuring standard compatibility. The 184 FEC redundancy bits are used as the amplitude bits of the MA-GMSK modulator. The corresponding amplitude bits of the AIS data packet overhead part are set to $x_n^{\mathrm{a}} = +1$. This results in transmitting the AIS data packet overhead part with high amplitude level in order not to impair synchronization. The 256 bits, which are fed as the amplitude bits into the the MA-GMSK modulator are depicted in Fig. 11.

B. Coding Schemes

We require a rate-1/2 systematic channel code for encoding the 184 data and CRC bits of an AIS data packet. Subsequently, we evaluate 2 different FEC schemes, namely the the 3rd Generation Partnership Project (3GPP) Long Term Evolution (LTE) turbo code [11] and a recursive terminated convolutional code.

1) Turbo Coding: We use the 3GPP LTE turbo code as specified in [11]. The LTE turbo code is a parallel concatenated convolutional coding scheme as shown in Fig. 12. It consists of two systematic recursive 8-state convolutional codes with

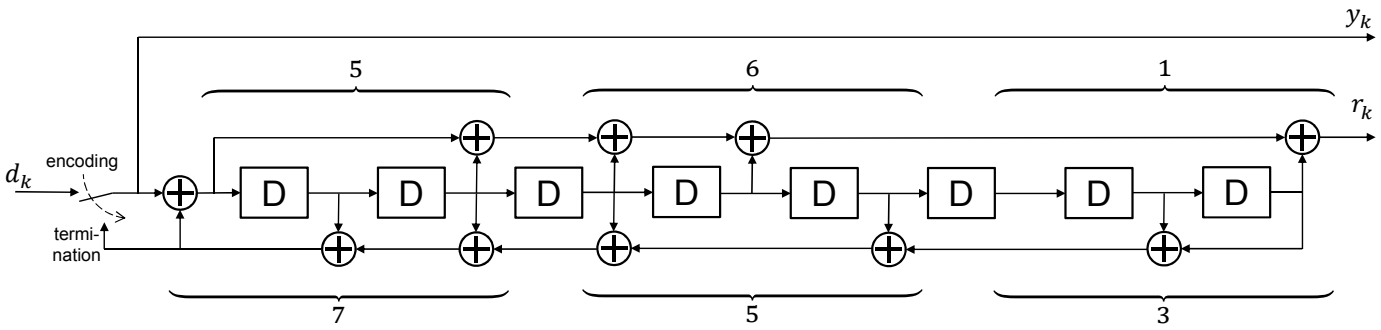

Fig. 13: Memory 8 recursive systematic convolutional encoder.

generator polynomials $(1, {}^{15}/_{13})$ in octal notation, an internal interleaver for parallel code concatenation and a rate matching and interleaving block.

The turbo encoder, shown in Fig. 12, starts with encoding the K data bits d_k with the switches in position "encoding", providing 3 bit streams $d_k^{(0)} = y_k = d_k$, $d_k^{(1)} = r_k$ and $d_k^{(2)} = r'_k$ for $k = 0, \ldots, K-1$. The initial states of the covolutional encoders, i.e., the memory blocks "D" are set to zero. Stream $d_k^{(0)}$ contains the data bits. $d_k^{(1)}$ and $d_k^{(2)}$ contain redundancy bits. After data encoding, the switches are changed to position "termination" for further 3 encoding clock cycles. This puts the convolutional encoders to zero state. The 3 termination cycles produce further 12 termination bits y_k, r_k, y'_k and r'_k, $k = K, \ldots, K+2$, which are appended to the bit streams as follows:

$$\mathbf{d}^{(0)} = \left[d_0, \ldots, d_{K-1}, y_K, r_{K+1}, y'_K, r'_{K+1}\right] \tag{26}$$

$$\mathbf{d}^{(1)} = \left[r_0, \ldots, r_{K-1}, r_K, y_{K+2}, r'_K, y'_{K+2}\right] \tag{27}$$

$$\mathbf{d}^{(2)} = \left[r'_0, \ldots, r'_{K-1}, y_{K+1}, r_{K+2}, y'_{K+1}, r'_{K+2}\right] \tag{28}$$

Each of these sequences $\mathbf{d}^{(i)}$ are interleaved by corresponding interleavers $\pi^{(i)}$.The interleaved sequences are denoted as

$$\mathbf{w}^{(i)} = \pi^{(i)}\left(\mathbf{d}^{(i)}\right), \qquad i = 1, 2, 3. \tag{29}$$

The turbo code word $\mathbf{c} = [c_0, \ldots, c_{N-1}]$ is constructed by aggregating the sequences $\mathbf{w}^{(i)}, i = 1, 2, 3$, where the bits of sequence $\mathbf{w}^{(0)}$ are the first $K+2$ bits of turbo code word $\mathbf{c}$. Interleaving, aggregation of the redundancy sequences $\mathbf{w}^{(1)}$ and $\mathbf{w}^{(2)}$ as well as matching the turbo code word length N for achieving a code rate of $R = {}^{K}/_{N}$ are described in [11].

Note the first $K+2$ bits of a turbo code word $\mathbf{c}$ contain the K data bits d_k in an interleaved order, defined by interleaver $\pi^{(0)}$. However, we require the data bits in unchanged order for standard compatible MA-GMSK. Therefore, we deinterleave the first $K+2$ turbo code bits, i.e., $\mathbf{w}^{(0)}$, using the inverse interleaver $\pi^{(0)\,-1}$. The first K bits of the deinterleaved sequence are the data bits d_k, which we use as phase bit input of the MA-GMSK modulator. For applying this coding scheme for encoding the data part of an AIS data packet, the number of data bits is $K = 184$ and the turbo code word length $N = 368$.

2) Convolutional Coding: Fig. 13 shows the block diagram of a 256-state (memory 8) recursive systematic convolutional code with generator polynomials $(1, {}^{561}/_{753})$ in octal notation. Encoding of K data bits d_k starts with the switch in position "encoding", providing 2 bit streams $y_k = d_k$ and r_k for $k = 0, \ldots, K-1$. The initial states of the memory blocks 'D' are set to zero. After data encoding, the switches are changed to position "termination" for further 8 encoding clock cycles. This puts the convolutional encoders to zero state and produces further 16 termination bits $y_K \ldots y_{K+7}$ and $r_K, \ldots r_{K+7}$. The $K+16$ redundancy and termination bits are interleaved by an interleaver π, which yields the sequence

$$\mathbf{w} = [w_0, \ldots, w_{K+15}] = \pi\left([y_K, y_{K+7}, r_0, \ldots, r_{K+7}]\right). \tag{30}$$

The first $N-K$ bits of sequence $\mathbf{w}$ build the redundancy part of the length-N convolutional code word

$$\mathbf{c} = [c_0, \ldots, c_{N-1}] = [d_0, \ldots, d_{K-1}, w_0, \ldots, w_{N-K-1}]. \tag{31}$$

The first $K = 184$ bits of the convolutional code word are the data bits d_k. We use them as phase bit input for standard compatible MA-GMSK modulation. The $N - K = 368 - 184 = 184$ redundancy bits are used as amplitude bit input of the MA-GMSK modulator.

VI. Numerical Results

In this section we evaluate the AIS packet error rate (PER) performance when applying multi-amplitude Gaussian minimum shift keying (MA-GMSK) modulation in combination with rate-1/2 forward error correction (FEC).

In a first step, we examine the AIS PERs when applying appropriate demodulation and decoding at an advanced AIS receiver. We do this examination by computer simulations.

In a second step, we investigate the packet error rate (PER) performance of common-off-the-shelf AIS receivers, which are fed with an multi-amplitude Gaussian minimum shift keying (MA-GMSK) signal. This investigation is done by laboratory measurements.

Fig. 14: Simulation block diagram for PER performance evaluation of MA-GMSK.

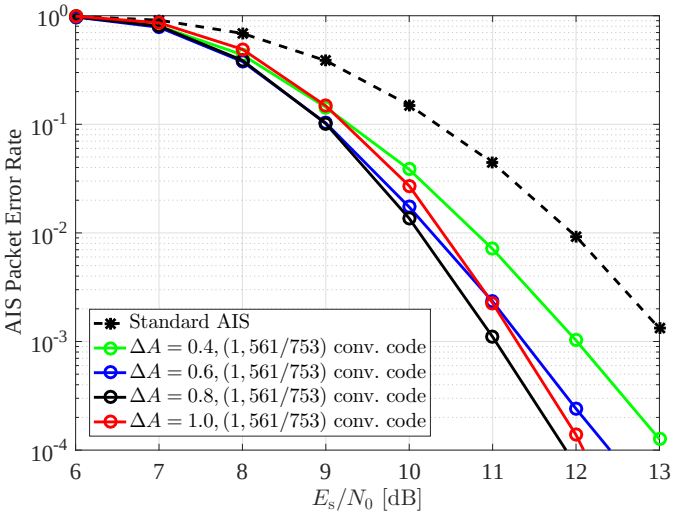

Fig. 15: AIS packet error rate (PER) versus E_s/N_0 for convolutional coded AIS data packets with MA-GMSK modulation.

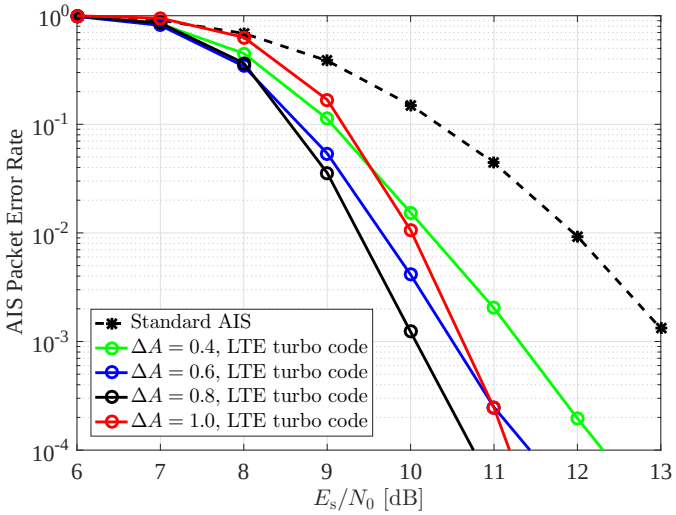

Fig. 16: AIS packet error rate (PER) versus E_s/N_0 for turbo coded AIS data packets with MA-GMSK modulation.

A. Simulations

We perform computer simulations for evaluation of the AIS packet error rate (PER) performance using an advanced receiver. The simulation block diagram is shown in Fig. 14.

At the transmitter side we generate AIS data packets as shown in Fig. 10. Out of an AIS packet we encode the 184 bits, consisting of 168 data bits and 16 CRC bits, using rate-1/2 systematic FEC. The 184 encoded bits itself appear unchanged at the encoder output. We use them as the *phase bits* at the MA-GMSK modulator input. These phase bits modulate the phase of the MA-GMSK baseband signal. The encoder provides 184 redundancy bits, which we use as *amplitude bits* for modulating the amplitude of the MA-GMSK baseband signal.

The advanced receiver applies MA-GMSK Max-Log-MAP demodulation as introduced in Sec. III. The MA-GMSK demodulator provides LLR values, which we use as (soft) input for the FEC decoder.

Fig. 15 shows the AIS PERs for different amplitude modulation coefficients ΔA when applying a systematic memory-8 convolutional code, which we have introduced in Sec. V-B2. The decoder applies maximum likelihood Viterbi decoding [12–14]. The PER of standard AIS, which uses uncoded GMSK modulation is shown as a reference. Compared to this reference, we observe a maximum SNR gain of approximately $1.3\,\mathrm{dB}$ for a amplitude modulation coefficient $\Delta A = 0.8$ at a PER of 10^{-1}. This coincides with the evaluation in Sec. IV, where we have observed maximum mutual information after demodulation for $\Delta A = 0.8$ as well. Assuming line-of-sight propagation with free space loss, an SNR gain of $1.3\,\mathrm{dB}$ corresponds to a gain in AIS transmission coverage, i.e., the maximum distance between transmitter and receiver, of $16.1\,\%$. With increasing SNR these gains further increase. At a PER of 10^{-3} we observe a maximum gain of about $2\,\mathrm{dB}$, corresponding to a gain in AIS transmission coverage of about $25.9\,\%$.

Fig. 16 shows the AIS PERs for different amplitude modulation coefficients ΔA when applying the 3GPP LTE turbo code. The decoder applies iterative Max-Log-MAP decoding [9,10,15] of the turbo component codes with 8 decoding iterations. Again, the PER of standard AIS is shown as a reference. Compared to memory-8 convolutional coding, the SNR gain further increases. We observe a maximum SNR gain of approximately $1.7\,\mathrm{dB}$ for a amplitude modulation coefficient $\Delta A = 0.8$ at a PER of 10^{-1}, which corresponds to a gain in AIS transmission coverage of about $21.6\,\%$. At a PER of 10^{-3} these gains increase to $3\,\mathrm{dB}$ and $41.3\,\%$ respectively. In general we observe, that the PER graphs' slope for turbo coding are steeper compared to convolutional coding.

During simulations we observed a similar computational complexity for decoding of the LTE turbo code and the memory-8 convolutional code.

B. Laboratory Measurements

Common-off-the-shelf AIS receivers expect a GMSK modulated radio signal as defined in [6]. Since AIS receivers have to

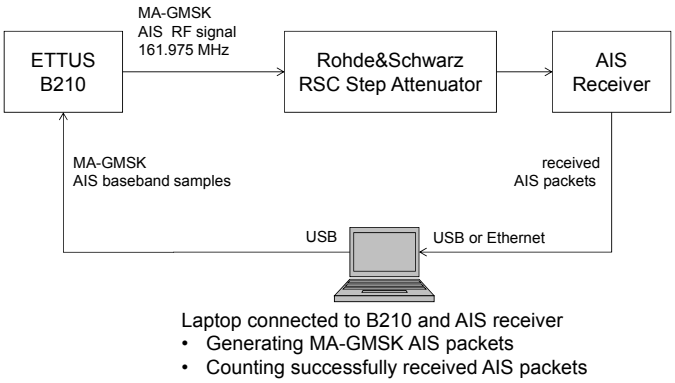

Fig. 17: Block diagram for the evaluation of the *Weatherdock Easy RX2* AIS receiver fed with MA-GMSK modulated radio signals.

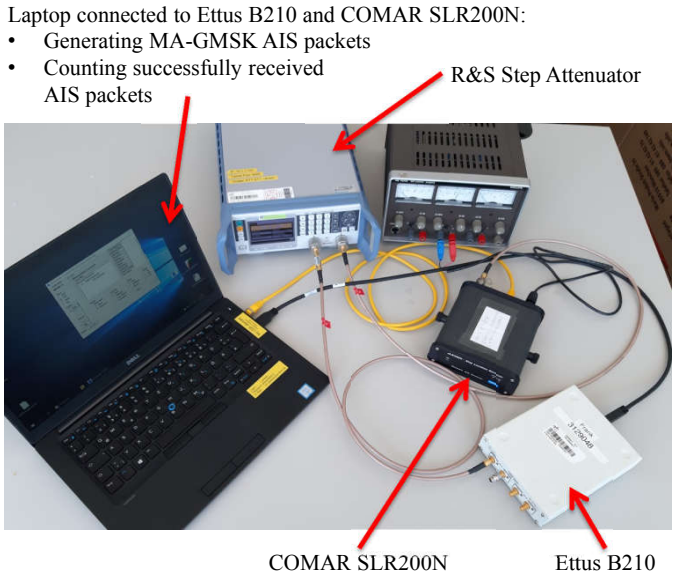

Fig. 18: Laboratory setup for the evaluation of the *COMAR SLR200N* AIS receiver fed with MA-GMSK modulated radio signals.

operate under dynamic signal propagation conditions, these receivers must be able to cope with signal amplitude fluctuations. With MA-GMSK we additionally introduce such amplitude fluctuations by modulation of the transmit signal's amplitude. It's necessary to show that common-off-the-shelf AIS receivers can cope with such additional amplitude modulation and detect AIS packets with the required sensitivity as defined in [6].

In this section, we investigate the PER performance of common-off-the-shelf AIS receivers, in particular the *COMAR SLR200N* and the *Weatherdock Easy RX2*, which we feed with an MA-GMSK modulated radio signal.

Fig. 17 shows the block diagram of the measurement setup. We use a laptop computer for generating MA-GMSK modulated AIS messages of type 1 (scheduled position report) in baseband. The baseband samples are transmitted via USB connection to an *Ettus B210* software defined radio. The software defined radio converts the baseband signal samples to passband at AIS channel A (161.975 MHz). A *Rohde&Schwarz RSC* step attenuator provides the MA-GMSK modulated radio signal to the AIS receiver under test at power levels ranging from $-120\,\mathrm{dBm}$ to $-80\,\mathrm{dBm}$. Fig. 18 shows a photo of the measurement setup for the *COMAR SLR200N* receiver.

For measuring PERs we count AIS packets, which are successfully detected by the AIS receiver under test. In total we transmit 1000 AIS packets and assume those who are not successfully received as erroneous. A packet transmission starts every $53.3\,\mathrm{ms}$, meaning that we use every second slot of an AIS TDMA frame.

Fig. 19 shows the AIS PERs for the *COMAR SLR200N* receiver. The MA-GMSK signal for $\Delta A = 0$ equals a GMSK signal. It's performance is plotted as reference. We observe that up to an amplitude modulation coefficient of $\Delta A = 0.6$, the *COMAR SLR200N* receiver provides a $20\,\%$ PER at $-108\,\mathrm{dBm}$, and therefore, still meets the sensitivity requirement as defined in [6], which states a $20\,\%$ PER at $-107\,\mathrm{dBm}$.

At higher amplitude modulation coefficients of $\Delta A > 0.6$ the AIS PER performance degrades clearly. This degradation

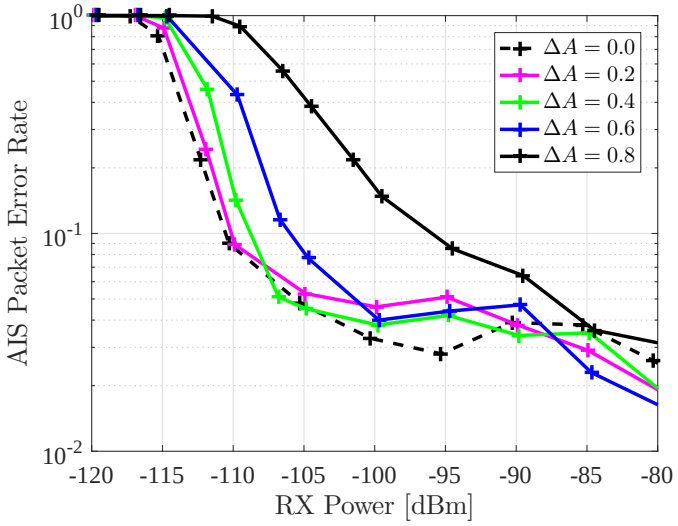

Fig. 19: packet error rates (PERs) for the *COMAR SLR200N* AIS receiver fed with an MA-GMSK signal containing AIS message type 1 data packets.

can in particular be observed for $\Delta A = 0.8$, which we previously have identified as a good choice for MA-GMSK in combination with FEC. In this case, the "low" amplitude level of MA-GMSK causes a significant transmit power reduction, so data bits, which are transmitted at "low" amplitude level, show a considerably higher error rate.

Fig. 20 shows the PERs obtained for the *Weatherdock Easy RX2* AIS receiver. This receiver also meets the sensitivity requirement up to an amplitude modulation coefficient of $\Delta A = 0.6$.

For both receivers, an amplitude modulation coefficient of $\Delta A = 0.4$ provides a PER performance close to the reference

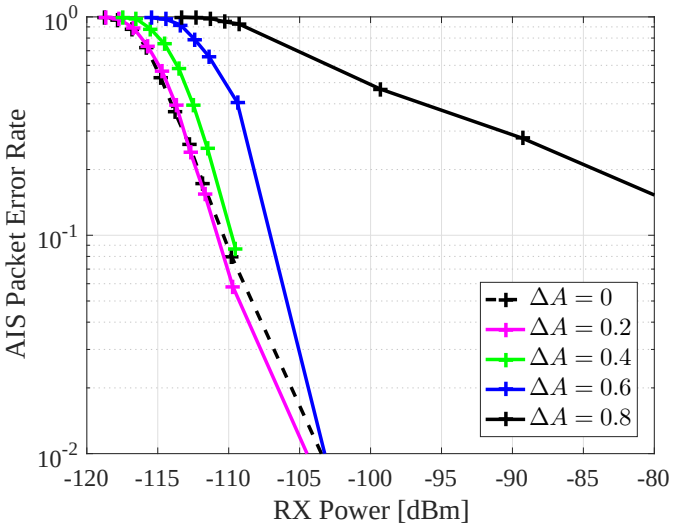

Fig. 20: packet error rates (PERs) for the *Weatherdock Easy RX2* AIS receiver fed with an MA-GMSK signal containing AIS message type 1 data packets.

reference of GMSK ($\Delta A = 0$), thus preserving the receivers' sensitivity margins.

VII. Summary and Conclusion

In this document, we have proposed a standard compatible forward error correction (FEC) extension for the Automatic Identification System (AIS). We have introduced binary multi-amplitude Gaussian minimum shift keying (MA-GMSK) modulation. The capability of transmitting additional bits via modulation of the amplitude of the original AIS Gaussian minimum shift keying (GMSK) signal is used to transmit redundancy bits of a FEC scheme. For FEC we have introduced systematic rate-1/2 channel codes, in particular the Long Term Evolution (LTE) turbo code and a memory-8 convolutional code.

Computer simulation results for the AIS packet error rate (PER) have shown signal-to-noise ratio (SNR) gains in the order of some decibels when applying the proposed standard compatible FEC schemes to the AIS. For verification of standard compatibility, we have investigated the PER performance of common-off-the-shelf AIS receivers, in particular the *COMAR SLR200N* and the *Weatherdock Easy RX2*, which we feed with an MA-GMSK modulated radio signal.

Based on simulation and measurement results, we propose an MA-GMSK amplitude modulation coefficient of $\Delta A = 0.4$. With this choice, common-off-the-shelf AIS receivers provide a PER performance close to the reference of GMSK ($\Delta A = 0$), thus preserving the receivers' sensitivity margins. At the same time performance improvements of an advanced receiver, applying FEC as proposed in this document, are still evident.

Appendix A
Measuring Mutual Information for Binary Data

In order to quantify information transfer, we are interested in measuring mutual information between bits, which we feed into a modulator at the transmitter side, and the corresponding outputs of the demodulator at the receiver side as shown in Fig. 21. We assume that the demodulator in Fig. 21 provides a soft decision value $L \in \mathbb{R}$ for the corresponding transmitted bit $x \in \{-1, +1\}$. For notational convenience, we omit the time index n at the moment. The mutual information between a transmitted bit x and the corresponding soft decision value L at the receiver side is defined as

$$\mathrm{I}(x;L) := \int_{-\infty}^{\infty} \sum_{x\in\{-1,+1\}} \mathrm{p}\left(x,L\right) \log_2 \frac{\mathrm{p}\left(x,L\right)}{\mathrm{p}(x)\ \mathrm{p}(L)}\ \mathrm{d}L, \quad (32)$$

where $\mathrm{p}\left(x,L\right)$ is the joint probability density function of the transmitted bit x and the corresponding soft decision value L. Using the definition of the conditional probability $\mathrm{p}\left(x|L\right)\ \mathrm{p}(L) = \mathrm{p}\left(x,L\right)$, marginal $\mathrm{p}(x) = \int \mathrm{p}\left(x,L\right)\ \mathrm{d}L$ and the logarithmic identities, we get

$$\mathrm{I}(x;L) = \overbrace{\sum_{x\in\{-1,+1\}} \mathrm{p}(x) \log_2 \frac{1}{\mathrm{p}(x)}}^{=\mathrm{H_b}(\mathrm{p}(x=+1))=\mathrm{H_b}(\mathrm{p}(x=-1))} - \int_{-\infty}^{\infty} \mathrm{p}(L) \underbrace{\sum_{x\in\{-1,+1\}} \mathrm{p}\left(x|L\right) \log_2 \frac{1}{\mathrm{p}\left(x|L\right)}}_{=\mathrm{H_b}(\mathrm{p}(x=+1|L))}\ \mathrm{d}L. \quad (33)$$

Due to binary transmission symbol alphabet $\{+1, -1\}$ we have $\mathrm{p}(x = -1) = 1 - \mathrm{p}(x = +1)$, respectively $\mathrm{p}\left(x = -1|L\right) = 1 - \mathrm{p}\left(x = +1|L\right)$. With that we use the definition of the binary entropy function [16]

$$\mathrm{H_b}(p) := p \log_2 \frac{1}{p} + (1-p) \log_2 \frac{1}{1-p} \quad (34)$$

to further simplify the notation of Eq. (33) and arrive at

$$\mathrm{I}(x;L) = \mathrm{H_b}(\mathrm{p}(x=+1)) - \underbrace{\int_{-\infty}^{\infty} \mathrm{p}(L)\, \mathrm{H_b}(\mathrm{p}\left(x=+1|L\right))\ \mathrm{d}L}_{=\mathrm{E}\{\mathrm{H_b}(\mathrm{p}(x=+1|L))\}}. \quad (35)$$

Note, for equally likely transmit symbols, i.e., $\mathrm{p}(x=-1) = \mathrm{p}(x=+1) = 0.5$, we get $\mathrm{H_b}(0.5) = 1$ for the first term in Eq. (35). The second term in Eq. (35) is the mean value of $\mathrm{H_b}(\mathrm{p}\left(x=+1|L\right))$ with respect to the probability density of the soft decision value L.

Assuming ergodicity, we can replace the mean value in Eq. (35) by averaging over a series of samples and get

$$\mathrm{I}(x;L) = \mathrm{H_b}(\mathrm{p}(x=+1)) - \lim_{N\to\infty} \frac{1}{N} \sum_{n=1}^{N} \mathrm{H_b}(\mathrm{p}\left(x_n=+1|L_n\right)). \quad (36)$$

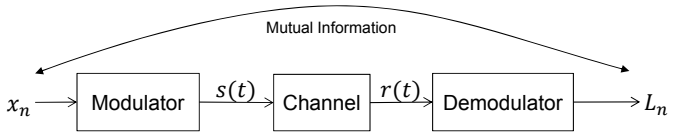

Fig. 21: Measuring mutual information between transmitted bits and demodulator output at the receiver.

Note, in practice we do not have available an infinite number of samples L_n. Thus, we cannot build the limit $N \to \infty$. If we omit building the limit, Eq. (36) is an approximation for the mutual information $\mathrm{I}(x; L)$.

In order to quantify the mutual information according to Eq. (36) we have to find a mathematical description of the conditional probability $\mathrm{p}\left(x_n = +1|L_n\right)$. We assume that the soft decision values L_n, which the demodulator shown in Fig. 21 provides, itself are log-likelihood ratios (LLRs). Therefore,

$$L_n = \ln \frac{\mathrm{p}\left(x_n = +1|L_n\right)}{\mathrm{p}\left(x_n = -1|L_n\right)} \tag{37}$$

according to the definition of a LLR. from Eq. (37) and with $\mathrm{p}\left(x_n = -1|L_n\right) = 1 - \mathrm{p}\left(x_n = +1|L_n\right)$ we get

$$\mathrm{p}\left(x_n = +1|L_n\right) = \frac{1}{1 + \mathrm{e}^{-L_n}}. \tag{38}$$

Inserting Eq. (38) into Eq. (36) we obtain

$$\mathrm{I}(x; L) = \mathrm{H_b}\left(\mathrm{p}(x = +1)\right) - \lim_{N\to\infty} \frac{1}{N} \sum_{n=1}^{N} \mathrm{H_b}\left(\frac{1}{1 + \mathrm{e}^{-L_n}}\right). \tag{39}$$

It is interesting to note that according to Eq. (39) we do not require the transmitted bit values for the calculation of the mutual information. It is sufficient to know the LLRs. Hagenauer already mentioned this nice property in [17], where he arrived at a slightly different but mathematically equivalent expression for the calculation of the mutual information between the transmitted bit and the corresponding LLR.

The calculation of the mutual information

$$\mathrm{I}(x; L) = \mathrm{H_b}\left(\mathrm{p}(x = +1)\right) - \lim_{N\to\infty} \frac{1}{N} \sum_{n=1}^{N} \mathrm{H_b}\left(\mathrm{Pe}_n\right). \tag{40}$$

in [17] is based on the bit error probability

$$\mathrm{Pe}_n = \frac{1}{1 + \mathrm{e}^{|L_n|}} = \frac{\mathrm{e}^{-|L_n|/2}}{\mathrm{e}^{-|L_n|/2} + \mathrm{e}^{|L_n|/2}} \tag{41}$$

of the transmitted bit x_n. This bit error probability can be calculated from the corresponding LLR L_n, in particular its magnitude, obtained at the receiver side. The equivalence of the solutions in Eq. (39) and [17] is evident from the symmetry of the binary entropy function, in particular $\mathrm{H_b}(p) = \mathrm{H_b}(1 - p)$, which leads to

$$\mathrm{H_b}\Bigg(\underbrace{\frac{1}{1 + \mathrm{e}^{-L_n}}}_{=p}\Bigg) = \mathrm{H_b}\Bigg(\underbrace{\frac{1}{1 + \mathrm{e}^{L_n}}}_{=1-p}\Bigg) = \mathrm{H_b}\Bigg(\underbrace{\frac{1}{1 + \mathrm{e}^{|L_n|}}}_{=p \text{ or } 1-p}\Bigg). \tag{42}$$

Consequently, the result of the binary entropy function does not depend on the sign of the LLR L_n. We can even use the LLRs' magnitudes $|L_n|$, which leads to the result in [17].

References

[1] *Digital cellular telecommunication system (Phase 2+); Physical layer on the radio path; (General description) (3GPP TS 05.01 version 8.9.0 Release 1999)*, European Telecommunications Standard Institute (ETSI), Jul. 2000, ETSI TS 100 573 V8.4.0. [Online]. Available: https://www.etsi.org/deliver/etsi_ts/100500_100599/100573/08.04.00_60/ts_100573v080400p.pdf

[2] *Digital cellular telecommunication system (Phase 2+); Modulation (GSM 05.04 version 7.1.1 Release 1998)*, European Telecommunications Standard Institute (ETSI), Jun. 2000, EN 300 959 V7.1.1. [Online]. Available: https://www.etsi.org/deliver/etsi_en/300900_300999/300959/07.01.01_60/en_300959v070101p.pdf

[3] *Digital Enhanced Cordless Telecommunications (DECT); Common Interface (CI); Part 2: Physical Layer (PHL)* , European Telecommunications Standard Institute (ETSI), Dec. 2019, ETSI EN 300 175-2 V2.8.1. [Online]. Available: https://www.etsi.org/deliver/etsi_en/300100_300199/30017502/02.08.01_60/en_30017502v020801p.pdf

[4] *DECT — The standard explained*, DECT Forum, Feb. 1997. [Online]. Available: https://www.dect.org/userfiles/file/General/DECT Background/DECT_Technical Document_1997.pdf

[5] *Bluetooth Core Specification*, Bluetooth SIG, Dec. 2019, v5.2. [Online]. Available: https://www.bluetooth.com/specifications/bluetooth-core-specification/

[6] *Technical Characteristics for an Automatic Identification System Using Time Division Multiple Access in the VHF maritime Mobile Frequency Band*, Radiocommunication Sector of the International Telecommunication Union (ITU-R), Feb. 2014, Recommendation ITU-R M.1371-5. [Online]. Available: https://www.itu.int/rec/R-REC-M.1371/en

[7] J. G. Proakis, *Digital Communications*, 3rd ed. McGraw-Hill, 1995, ISBN 0-07-051726-6.

[8] G. Stüber, *Principles of Mobile Communication*. Springer International Publishing, 2017. [Online]. Available: https://books.google.de/books?id=cSYmDwAAQBAJ

[9] L. Bahl, J. Cocke, F. Jelinek, and J. Raviv, "Optimal decoding of linear codes for minimizing symbol error rate," *IEEE Transactions on Information Theory*, vol. 20, no. 2, pp. 284–287, Mar. 1974.

[10] P. Robertson, E. Villebrun, and P. Höher, "A comparison of optimal and sub-optimal MAP decoding algorithms operating in the log domain," in *Proceedings IEEE International Conference on Communications (ICC 1995), Seattle, USA*, vol. 2, Jun. 1995, pp. 1009–1013.

[11] *LTE; Evolved Universal Terrestrial Radio Access (E-UTRA); Multiplexing and channel coding (3GPP TS 36.212 version 8.7.0 Release 8)*, ETSI, Jun. 2009, ETSI TS 136 212 V8.7.0.

[12] A. J. Viterbi, "Error bounds for convolutional codes and an asymptotically optimum decoding algorithm," *IEEE Transactions on Information Theory*, vol. 13, no. 2, pp. 260–269, Apr. 1967.

[13] G. D. Forney, "The Viterbi algorithm," *Proceedings of the IEEE*, vol. 61, no. 3, pp. 268–278, 1973.

[14] A. J. Viterbi, "A personal history of the Viterbi algorithm," *IEEE Signal Processing Magazine*, vol. 23, no. 4, pp. 120–142, Jul. 2006.

[15] C. Berrou, A. Glavieux, and P. Thitimajshima, "Near Shannon limit error-correcting coding and decoding: Turbo-codes," in *Proceedings of ICC '93 - IEEE International Conference on Communications*, vol. 2, 1993, pp. 1064–1070.

[16] D. J. C. MacKay, *Information Theory, Inference & Learning Algorithms*. Cambridge University Press, 2005, fourth printing. [Online]. Available: https://www.inference.org.uk/itprnn/book.pdf

[17] J. Hagenauer, "The EXIT chart — introduction to extrinsic information transfer in iterative processing," in *European Signal Processing Conference (EUSIPCO)*, 2004.